ChemPubSoc Europe

DOI: 10.1002/chem.201700078

CHEMISTRY A European Journal Full Paper

Zeolites | *Hot Paper*

Probing Zeolite Crystal Architecture and Structural Imperfections using Differently Sized Fluorescent Organic Probe Molecules

Frank C. Hendriks,[a] Joel E. Schmidt,[a] Jeroen A. Rombouts,[b] Koop Lammertsma,[b] Pieter C. A. Bruijnincx,[a] and Bert M. Weckhuysen*[a]

Abstract: A micro-spectroscopic method has been developed to probe the accessibility of zeolite crystals using a series of fluorescent 4-(4-diethylaminostyryl)-1-methylpyridinium iodide (DAMPI) probes of increasing molecular size. Staining large zeolite crystals with MFI (ZSM-5) topology and subsequent mapping of the resulting fluorescence using confocal fluorescence microscopy reveal differences in structural integrity: the 90° intergrowth sections of MFI crystals are prone to develop structural imperfections, which act as entrance routes for the probes into the zeolite crystal. Polarization-dependent measurements provide evidence for the probe molecule's alignment within the MFI zeolite pore system. The developed method was extended to BEA (Beta) crystals, showing that the previously observed hourglass pattern is a general feature of BEA crystals with this morphology. Furthermore, the probes can accurately identify at which crystal faces of BEA straight or sinusoidal pores open to the surface. The results show this method can spatially resolve the architecture-dependent internal pore structure of microporous materials, which is difficult to assess using other characterization techniques such as X-ray diffraction.

Introduction

Zeolites, crystalline microporous materials constructed of a 3D network of silica and alumina tetrahedra, are the most widely used heterogeneous catalysts in the chemical industry.[1] Factors contributing to this success are their excellent chemical and hydrothermal stability, well-defined structure, and large surface area. Zeolites are traditionally used in major (petro-)chemical processes, such as hydrocracking and catalytic cracking,[2,3] as well as more recently in biomass conversion.[4–6] Their widespread use motivates research into a proper understanding of the structure and behavior of these materials, as improvements have a large impact given the scale at which they are applied.[7,8] The microporous structure of zeolites influences their reactivity, so location-specific information on a microscopic scale is important to elucidate structure–property relationships. However, due to the size of zeolite particles used in shaped catalyst bodies, such as extrudates, often as small polycrystalline particles or small crystals, this information can be very difficult to obtain.

Large, micron-sized zeolite crystals are often used in micro-spectroscopic studies[9–11] because their size and regular three-dimensional structure allows for a more precise evaluation of the location of guest molecules[12,13] and active sites[14] in discrete areas of the zeolite crystal. The structural features of such zeolite crystals can be used to determine structure–property relationships; the knowledge gained can then be applied to industrially relevant zeolite powders.[15,16] From these large zeolite crystal studies, it is found that seemingly homogeneous crystals actually exist as complex crystalline intergrowths.[17] In addition, zeolite crystals can have structural defects[18] or intentionally created mesopores, influencing both the accessibility as well as the rate and extent of adsorption of molecules. These heterogeneities and changes in internal architecture complicate the structure, can create internal diffusion barriers and can give rise to gradients of catalytically active heteroatoms.[19] Therefore, understanding structure–activity relationships in zeolite crystals is vital to the optimization of properties of these crystals and the knowledge gained can be translated to zeolite-containing catalysts.

The use of probe molecules and probe reactions has been indispensable in the study of large zeolite crystals. Studying the accessibility and reactivity of small molecules can provide a wealth of information on the pore network of zeolites and their active sites.[20] Well-known examples include probing the accessibility of zeolites using gases[21] and the study of zeolite

[a] F. C. Hendriks, Dr. J. E. Schmidt, Dr. P. C. A. Bruijnincx, Prof. Dr. B. M. Weckhuysen
Inorganic Chemistry and Catalysis
Debye Institute for Nanomaterials Science, Utrecht University
Universiteitsweg 99, 3584CG Utrecht (The Netherlands)
E-mail: b.m.weckhuysen@uu.nl

[b] J. A. Rombouts, Prof. Dr. K. Lammertsma
Department of Chemistry and Pharmaceutical Sciences
VU University Amsterdam, De Boelelaan 1083
1081 HV Amsterdam (The Netherlands)

Supporting information and the ORCID numbers for the authors of this article can be found under: http://dx.doi.org/10.1002/chem.201700078.

© 2017 The Authors. Published by Wiley-VCH Verlag GmbH & Co. KGaA. This is an open access article under the terms of Creative Commons Attribution NonCommercial License, which permits use, distribution and reproduction in any medium, provided the original work is properly cited and is not used for commercial purposes.

acidity by oligomerization of styrene derivatives,[14,22] thiophene derivatives,[23] or furfuryl alcohol.[10,24,25] The regular pore system of zeolite crystals can be exploited in polarization dependent measurements in which the alignment of probe reaction products within the pore system can be used to gain more insight in the location and orientation of these molecules in porous catalytic solids.[26,27]

Previously, we have reported on the accessibility of zeolite powders using a series of rod-shaped probe molecules of tunable size, based on the 4-(4-diethylaminostyryl)-1-methylpyridinium iodide (DAMPI) scaffold.[28] Advantageously, this probe only exhibits fluorescence if positioned in a confined environment, such as a zeolite pore, with fluorescence in solution being fully quenched by *cis–trans* isomerization.[17] Furthermore, it is one of the smallest fluorescent probe molecules available that does not require external activation (i.e., a reaction that produces a fluorescent species), allowing a wide range of microporous materials to be probed. By combining DAMPI probe molecules of different sizes with zeolite frameworks containing varying pore apertures, the diameter of the probes was found to correlate with both the accessibility to and the rate of adsorption into the zeolite pore network. DAMPI probes have also been successfully used in studying internal diffusion barriers arising from intergrowths in zeolite crystals,[19] as well as the change in accessibility of steamed zeolites due to mesopore formation.[30]

Here, we use a series of fluorescent DAMPI-derived probe molecules of increasing diameter to test the accessibility of micropores, structural imperfections, as well as the micropore orientation of large zeolite crystals. We focus on two industrially relevant zeolite materials, namely MFI (ZSM-5, with 10-membered rings) and BEA (Beta, with 12-membered rings). The method provided allows one to study complete crystals and to non-destructively probe their interior. Moreover, that no reaction is needed to create fluorescent species means that silicalite and other non-reactive microporous material compositions can be probed as well. The anisotropy of the rod-shaped probe molecules is exploited in polarization-dependent confocal fluorescence microscopy (CFM) experiments showing the alignment of probe molecules in the zeolite pore network, thus revealing the pore orientation of the two distinct zeolite crystals under study.

Results and Discussion

Zeolite crystal architecture, molecular probes, and fluorescence microscopy

As shown in Figure 1 a, large ZSM-5 crystals with typical dimensions of 100×20×20 μm were used as a model for zeolite MFI. These zeolite crystals have been the subject of many studies, providing detailed knowledge of their internal structure and composition.[14,17,19] It has been demonstrated that these materials are not single crystals, but rather consist of two types of subunits with distinct shapes (Figure 1 c) and that intra-crystalline voids are present between these subunits due to an

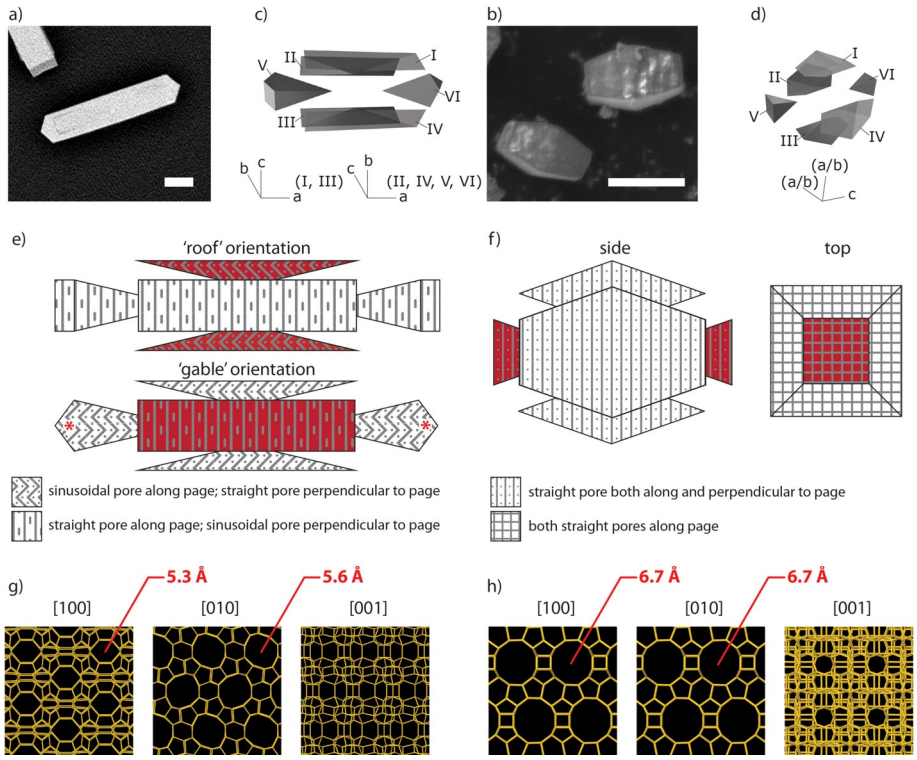

Figure 1. Overview of the two zeolite framework topologies used in this study. a, b) SEM images of zeolite MFI (a) and zeolite BEA (b) crystals; the scale bars represent 20 μm. c, d) Schematic representation of the zeolite crystals showing the different subunits of which the crystals consist. The directions of the crystallographic edges for the subunits are shown below the model. e, f) Schematic representation of both the zeolite crystals showing the pore orientation in plane and parallel to the plane. Subunits with a high concentration of imperfections are shown in red for each zeolite crystal (vide infra). g, h) View of the zeolite framework along [100], [010], and [001], showing the pores that surface at those faces.[29].

© 2017 The Authors. Published by Wiley-VCH Verlag GmbH & Co. KGaA, Weinheim

imperfect match of the subunit's interface.[19,31] MFI has a 3D pore system with straight pores opening to the [010] face and sinusoidal pores opening to the [100] face, as shown in Figure 1e. The 10-membered ring pores have pore diameters between 5.3 and 5.6 Å (Figure 1g). The growth mechanism of these zeolite crystals causes a 90° rotational intergrowth for subunit I and III, as evidenced by electron backscatter diffraction.[19] This intergrowth has been shown to introduce structural weakness particularly to these subunits.[17] Thus, the direction of the sinusoidal and straight pores is switched in subunits I and III compared to the rest of the crystal. It is important to note that, regardless of the subunit, both the sinusoidal and straight pores of these large MFI crystals lie in the direction of the short axes of the crystal (i.e., never along the long axis).

The typical dimensions of the BEA crystals used in this work are 20×10×10 μm (Figure 1b), which is similar to the BEA crystals typically used in sugar isomerization experiments, one of the promising applications of BEA materials.[32] The crystals have a truncated bipyramidal morphology, typical for crystals synthesized in this way.[33] An hourglass pattern similar to that of MFI crystals has been reported for much larger crystals (ca. 400 μm) of this type, but has not yet been demonstrated in smaller crystals.[34] BEA has a 12-membered ring 3D pore system, with large 6.7 Å pores opening to the [100] and [010] face (Figure 1h). Sinusoidal pores open to the [001] face; these types of pores have a smaller effective diameter due to their zig-zag shape. Previous results from XRD measurements on the aforementioned 400 μm-large BEA crystals showed that the [001] face is at the short, square end of the crystal.[34] Consequently, the straight pores open to all of the faces on the long sides of the crystal.[35] The structure of BEA is complicated by the fact that multiple, intergrown polymorphs, namely A and B, can be formed.[34,36–38] There is virtually no preference in growth of these polymorphs, which leads to layers of polymorphs on top of each other, making crystallographic analysis of zeolite BEA crystals rather difficult.[39] Moreover, these stacking faults also further restrict movement through the sinusoidal pores. The zeolite BEA crystals used in this study were synthesized using fluoride, which usually leads to highly crystalline, defect-free crystals. Contrary to MFI crystals in this study, to the best of our knowledge, the crystal morphology of BEA crystals has not been investigated in significant detail. Notably, and also in contrast to the MFI crystals, the crystals used here are free of aluminium and thus contain no strong Brønsted acid sites.

The accessibility of probe molecules in the zeolite pore network and structural imperfections, such as cracks, of these two types of large zeolite crystals was evaluated using a series of fluorescent DAMPI-based probe molecules with increasingly bulky alkyl substituents.[28] These probe molecules, denoted as **1**–**4**, are depicted in Figure 2 together with their dimensions and spectroscopic properties. The steric bulk is increased by changing the *N*-alkyl substituents from methyl to cyclohexyl substituents, with the larger substituents giving the molecule a distinct T-shape. Based on their sizes (varying from 5.8 for **1** to 10.1 Å for **4**), probe molecule **1** is expected to be able to

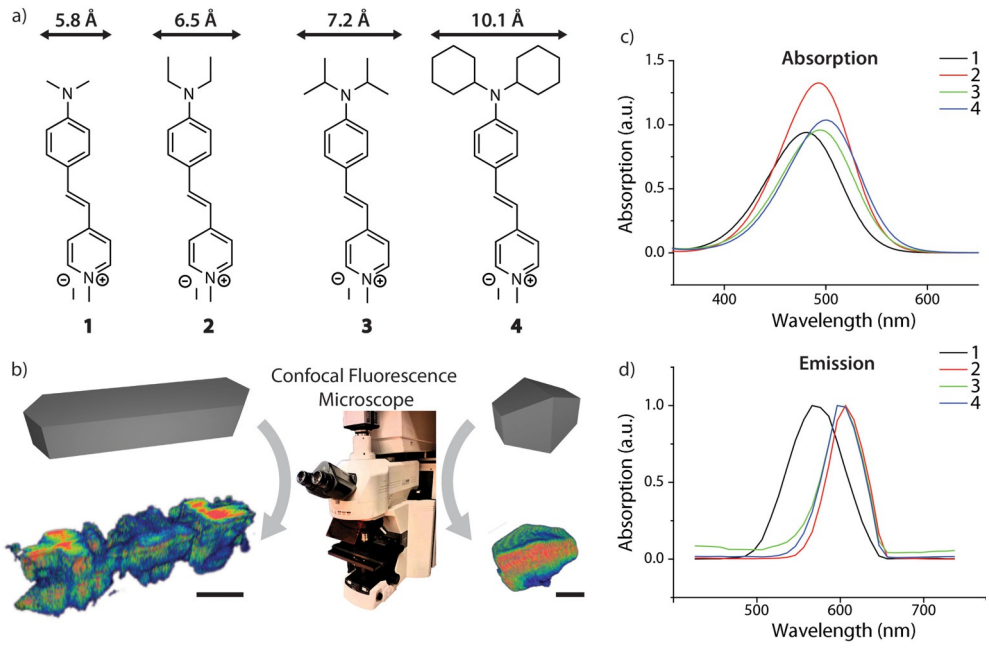

Figure 2. An overview of the experimental approach taken in this work. a) Molecular probes **1**–**4** used in this research. The width of the probe molecule is calculated by fitting the smallest enclosing cylinder around the optimized structure as calculated by Density Functional Theory (DFT).[28] b) Schematic model of a zeolite MFI crystal (left) and a zeolite BEA crystal (right) with 3D confocal fluorescence microscopy maps for both zeolite crystals after staining with probe molecule **1**. The 3D images were obtained by stacking of individual fluorescence microscopy maps using alfa blending mode. Different settings were used for the zeolite MFI and BEA crystals so the absolute intensities cannot be compared. The scale bars represent 20 μm. c) Absorption spectra of probe molecules **1**–**4** in equimolar solutions in ethanol. At the absorption maximum, the extinction coefficients of the probes are 37.6×10^3, 53.1×10^3, 38.3×10^3, and 41.5×10^3 M^{-1} cm^{-1} for probe **1**–**4**, respectively. d) Normalized emission spectra of probe molecules **1**–**4**, recorded by confocal fluorescence microscopy on the pure compounds in solid form.

© 2017 The Authors. Published by Wiley-VCH Verlag GmbH & Co. KGaA, Weinheim

enter the pores of zeolite MFI, whereas probe molecules **1** and **2** are expected to be able to enter the pores of zeolite BEA.

The ability of the molecular probes to enter the zeolite pores was examined by evaluating probe uptake by the zeolite crystals from solution. Crystals of zeolites BEA and MFI were submersed in solutions of the probes until equilibrium was reached, after which they were collected, washed (in the case of MFI) and examined by CFM. The fluorescence of zeolite MFI crystals did not change after repeatedly washing with ethanol, suggesting that the probe is strongly bound, most likely to the Brønsted acid sites of the zeolite.[28] For zeolite BEA, however, washing of the crystals after staining lowered the fluorescence significantly, indicating that the probes are not strongly bound to the zeolite, as expected, given the lack of Brønsted acid sites in this sample. Therefore, zeolite crystals with BEA morphology were not washed after staining. Visible inspection of the zeolite crystals after staining showed that for both types of crystals, probe molecule **1** caused the zeolite crystals to become bright pink, whereas probe molecules **2**–**4** did not induce a color change. In the CFM experiments, only isolated single crystals were considered. It was confirmed visually that the zeolite crystals were undamaged, but no selection was performed based on the observed fluorescence.

The laser light source of CFM is intrinsically polarized, allowing for polarization-dependent measurements to be carried out on probe molecule **1** in both zeolite MFI and BEA crystals. Experimentally, the zeolite crystals were rotated with respect to the angle of polarization of the incoming laser light. The conjugated chromophore of the DAMPI scaffold runs along the long axis of the molecule, causing anisotropic light absorption. Therefore, the DAMPI-type probe molecules used in this work will absorb (and emit) light only when specifically oriented with respect to the incident laser light polarization. Time-dependent DFT (TDDFT) calculations showed that light absorption is maximized when the molecule's Y axis (Figure 3) is oriented perpendicular to the incoming laser light (i.e., parallel to the microscope table) and parallel to the polarization axis of the light. If the molecule is rotated away from the orientation of maximum absorption, absorption gradually decreases. As is shown in Figure 3, light polarized along the X and Z axes is not absorbed by the molecule. Polarization-dependent CFM measurements thus directly give the orientation of the long axis of the molecule. The observed polarization dependency, shown in Figures 4 and 6, demonstrates that most of the molecules are aligned, indicating that the molecules have entered and are aligned in the micropores of the zeolite crystal; the angle of polarization is indicated by arrows in these figures.

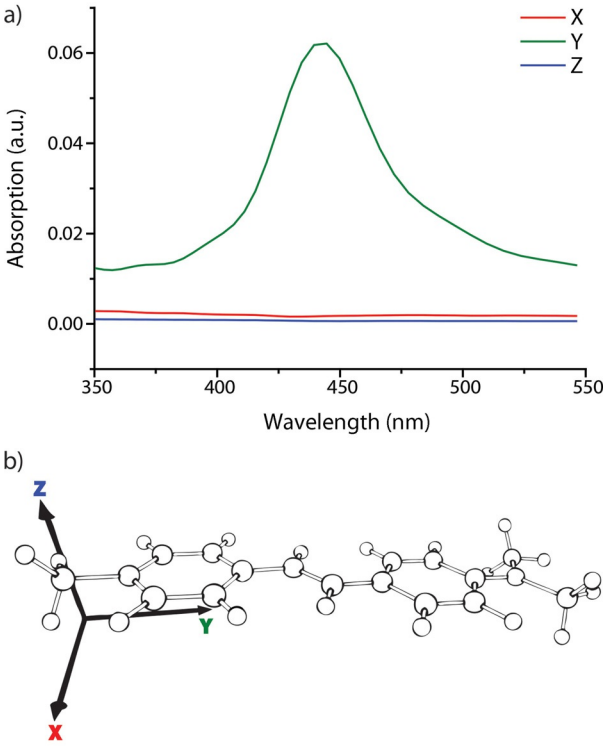

Figure 3. Polarization dependence of the absorption of probe molecule **1** with respect to laser light polarization. Graph a) shows the absorption of light of probe molecule **1** if the angle of light polarization is parallel to the axis X, Y, or Z; the propagation direction of light is then perpendicular to that axis. The absorption was calculated by TDDFT. Light absorption is at maximum when light polarization is parallel to the probe's long axis (Y) and thus propagates in any direction in the XZ plane. The λ_{max} of the absorption band is found at a lower wavelength compared to the experimental value, which is common for TDDFT.[40] The b) diagram shows the axes used in the calculation of the polarization dependence.

Micro-spectroscopic investigation of zeolite MFI crystals

Figure 4a shows that the fluorescence of the zeolite MFI crystals stained with the probe molecules is not distributed homogeneously throughout the crystal. More specifically, an hourglass pattern is visible, similar to how the (unstained) crystal looks when examined under crossed polarizers.[41,42] The aforementioned space between the subunits of the zeolite crystals must therefore provide access to the interior of the crystal, which allows the probe molecules to enter. The hourglass pattern is a recurring feature in virtually all of the studied crystals (see also Figure S1 in the Supporting Information), but for each probe, the intensity of the pattern differs. From the low amount of fluorescence observed in these areas for the larger probe molecules, it can be concluded that the limited opening between the subunits is not much larger than the largest probe.

When deposited on a flat surface (i.e., the microscope table), the zeolite crystals are encountered in two orientations in equal amounts: the "gable" and "roof" orientation.[14] Looking at the distribution of fluorescence for probe molecule **1** throughout the crystal, the two orientations of the crystal show distinct differences. In the roof orientation, the fluorescence observed has the shape of an hourglass, whereas in the gable orientation, fluorescence is observed in a rectangular area (Figure 4). From these observations, it can be concluded that in both orientations, the fluorescence is originating from the same subunits, namely subunits I and III (marked red in Figure 1e). The other subunits of the zeolite crystal only show a small amount of fluorescence at the edges.

© 2017 The Authors. Published by Wiley-VCH Verlag GmbH & Co. KGaA, Weinheim

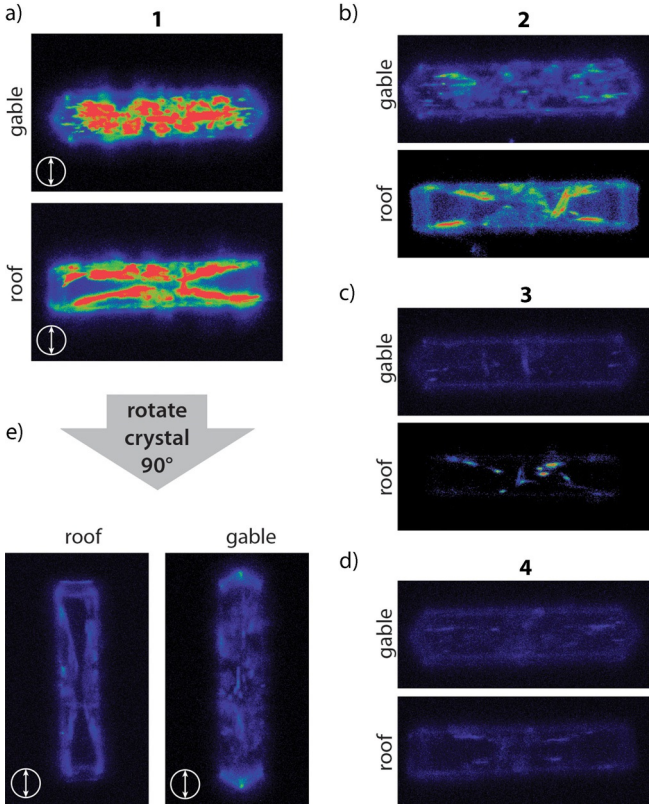

Figure 4. Fluorescence location in zeolite MFI crystals. The experimental settings were kept constant in all CFM images presented in this figure. a–d) Summed intensity over all layers of 3D maps of the zeolite crystals stained with probe molecules **1** (a), **2** (b), **3** (c), and **4** (d) in the two possible orientations of the zeolite crystals: "gable" (top) and "roof" (bottom) orientation. e) Image of zeolite MFI crystal after the crystal has been physically rotated by 90°, that is, with respect to the angle of polarization of the incoming laser light, showing diminished fluorescence intensity for both orientations.

Examining the size of each probe molecules with respect to the MFI pore size reveals that only **1** can enter the zeolite micropore system.[28] The bulky side groups of the other probes allow only partial, end-on entrance into the pore mouths. The only area on the crystal exterior where straight pores surface are the faces designated by a star in Figure 1e. To evaluate the penetration of probe molecules of **1** into straight pores of the crystal, one should therefore look at the 'roof" orientation: in this orientation, the molecules that have entered the straight pores through the area marked with a star will be oriented to maximize absorption of laser light (see Figure 3). From the fluorescence maps, it is clear no additional fluorescence is observed in this area. Thus, movement through straight pores is very slow, presumably because of the tight fit between probe and zeolite. From this result, it is clear that movement through straight pores cannot account for the fluorescence observed in crystals stained with **1**.

The highly fluorescent nature of subunits I and III coincides with the different crystallographic orientation in these subunits with respect to the other units due to the 90° intergrowth in the crystal. In both orientations, fluorescence is distributed heterogeneously throughout these subunits and fluorescence intensity varies between subunits and between crystals (Figure S1). It is known that rotational intergrowths can induce structural weakness in zeolite crystals. Roeffaers et al.[17] have shown that intentionally damaging the crystal by sudden temperature changes allows probe molecule **2** to enter the subunits of the zeolite crystal. The crystals used in this study were calcined very gently according to methods used previously;[17] it is therefore unlikely that the calcination procedure damaged the crystals to a large extent. Therefore, the fluorescence results suggest that there must be many imperfections within subunits I and III, which allow the smaller probe molecule **1** to enter. A comparison of the fluorescence of zeolite MFI crystals stained with probe molecules **1**–**4** shows intense fluorescence for **1** and only little fluorescence for **2**–**4**. This result is similar to what has been observed in experiments with the same probes in MFI zeolite powder.[28] In the fluorescence maps of each probe molecule, outlines of fluorescence can be observed at the edges of the crystal, which suggests the probes are inserted end-on into the sinusoidal pore mouths at the surface in a "stopcock" fashion, as previously proposed by Roeffaers et al.[9,17]

Although the CFM images shown in Figure 4 are representative for most of the zeolite MFI crystals stained with probe molecules **1**–**4**, it should be noted that there is considerable heterogeneity in fluorescence intensity between the different MFI crystals stained with the same probe molecule. A warning against the assumption of homogeneity of crystal properties within the same batch has also been issued recently.[43] Therefore, to eliminate any experimenter's bias, we evaluated the intensity for eight of these MFI crystals stained with probe molecules **1**–**4**. In this way, a comparison could be made of the amounts of each probe molecule taken up by the zeolite crystals. The total fluorescence intensity for each zeolite crystal was summed over the entire crystal and evaluated for each type of probe molecule. Probe molecule concentrations for each type of probe molecule are compared in Figure 5. Significant differences (>95% confidence, see Table S1) in average fluorescence intensity were found for the probe molecules, regardless of the differences in intensity seen for different crystals using the same probe. The only exceptions to this for MFI crystals are probes **3** and **4**, for which the differences in average intensity were too small. This approach shows the feasibility of using this series of fluorescent probe molecule experiments with consistent results on zeolite crystals, even though the fluorescence observed seems heterogeneous. The clear differences in fluorescence intensity between crystals stained with differently sized probes offer a unique way to measure the accessibility of the crystal to molecules of discrete sizes.

The polarization dependence of zeolite MFI crystals stained with probe molecule **1** is shown in Figure 4e. It was found that the fluorescence intensity is the highest when the light polarization is parallel to the short axis of the crystal, whereas a rotation of 90° leads to an almost complete disappearance of fluorescence. Both roof and gable orientations show this behavior. The large differences in fluorescence upon rotation of the crystal show that most of the probe molecules are aligned relative to each other, meaning they are aligned in identical micropores of the zeolite, shown in Figure 5. Interestingly,

© 2017 The Authors. Published by Wiley-VCH Verlag GmbH & Co. KGaA, Weinheim

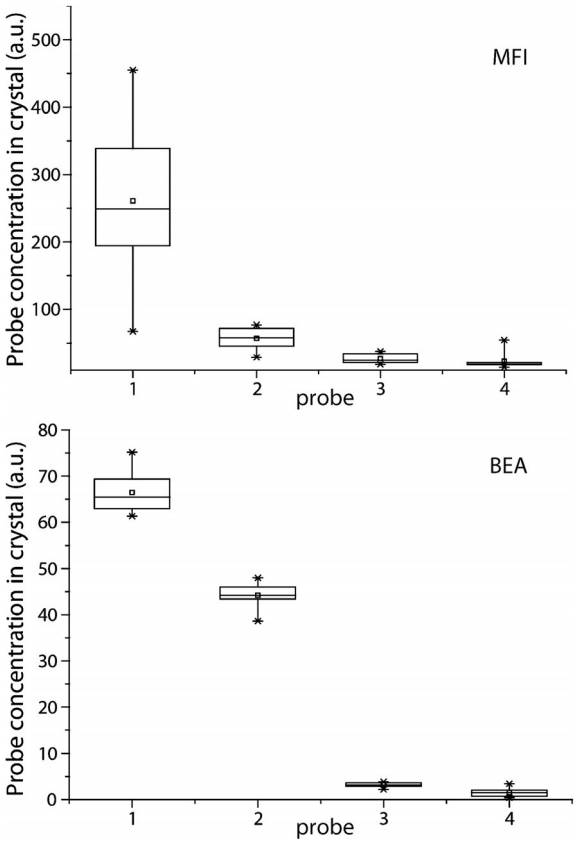

Figure 5. Overview of the total fluorescence intensities of zeolite MFI and BEA crystals after staining with probe molecules **1**–**4**. For each probe, background-corrected fluorescence was summed over all layers of a 3D map of the crystal and corrected for differences in extinction coefficient of the probe. The box plot signifies all data for each probe. Eight zeolite crystals were evaluated for each probe and each type of crystal to obtain statistically significant results. Intensities between the both types of zeolite crystals were taken using different measurement settings and should therefore not be compared.

probe molecules **2**–**4** also exhibit polarization-dependent behavior, with a similar maximum and minimum upon rotation of the crystal (Figure S3). This implies that even though the other probe molecules are unable to enter the pore system because of their size, they are still aligned to the pore system in a regular fashion. Although the steric bulk of these probe molecules precludes full entry into the pores, part of the probe molecule may insert itself into the pore mouth of the zeolite end-on in a "stopcock" fashion. This result suggests that probe molecules can be visualized selectively at the pore mouth of the zeolite crystal, a location of particular interest for catalysis.[9,44] For example, these probes may be used to detect pore blockage at the surface.[45] Rotating the zeolite crystal at 30° intervals, shown in Figure 7, demonstrates that the fluorescence intensity follows a $\sin(2\Theta)$ curve.[46] The small overall decrease in fluorescence intensity upon multiple rotations is caused by photobleaching of the probe molecules upon prolonged exposure to laser light (i.e., after multiple measurements of the same zeolite crystal).

Interestingly, for both "gable" and "roof" orientations, fluorescence is observed almost exclusively in subunits I and III. The pore orientation of MFI crystals, as elucidated in previous studies,[19,26,47] dictates that for subunits I–IV, straight pores run parallel to the crystal outer surface. The fluorescence originating from I and III in the gable orientation therefore indicates that probe molecule **1** is aligned to the straight pores of these subunits. This is expected because probe **1** fits into the straight pores of MFI.[28] In the roof orientation, however, the same rationale leads to the conclusion that probe molecule **1** must be aligned to the sinusoidal pores of the crystal. This counterintuitive result can be explained by the many imperfections in these subunits. It is possible that the deterioration in pore structure could make the sinusoidal pores wider and accessible to probe molecules. However, from the observed polarization dependence of the fluorescence, it follows that the probes are still aligned to the direction of the pore; thus, there is no complete breakdown of pore structure. In this way, subunits I and III have probe molecule **1** in both types of pores. In the gable orientation, the probes in the straight pores are visible, whereas in the roof orientation, the probes in the sinusoidal pores are visible.

Micro-spectroscopic investigation of zeolite BEA crystals

BEA crystals stained with probe molecule **1** or **2** show fluorescence distributed throughout the complete crystal (Figure 6 and Figure S2 in the Supporting Information). Based on their size, both probes should be able to enter the zeolite pore system and be distributed throughout the crystal. In contrast, probe molecule **3** shows fluorescence mostly at the edges of the BEA crystal. Indeed, given its size, probe molecule **3** is not expected to be able to enter the pores of the BEA crystal, and is present at the entrance of the pores. Some irregular fluorescence is observed for probe molecule **3**; however, this is more pronounced for probe **4,** for which randomly distributed areas within the crystal show fluorescence intensity. Probe molecule **4** is also present at the edges of the crystal, but the fluorescence is very weak (see Figure S2). These results suggest that probe molecule **4** (and also probe **3**, which is less visible due to fluorescence at the edges) can enter and stain imperfections of the crystal (see Figure S2). In this way, probe molecule **4** can effectively be used to detect cracks and structural imperfections in the crystals that are accessible from the outside of the BEA crystal.

In analogy to MFI crystals, fluorescence intensity was evaluated for several BEA crystals to compare the difference in uptake of the probes. The results are summarized in Figure 5. Probe molecule **1** shows the highest concentration in BEA, followed by probe **2**, whereas **3** and **4** are taken up in very minor amounts. This is in agreement with the sizes of the probe molecules with respect to the pore size of BEA. From the box plots, it is apparent that there is considerably less spread in fluorescence intensity between zeolite BEA crystals stained with the same probe, which is the case for MFI. The very consistent fluorescence intensity of these crystals per probe should be attributed to the low number of defects in these crystals, as a result of the fluoride-assisted synthesis method. For probe molecule **4**, low fluorescence intensity is observed,

 © 2017 The Authors. Published by Wiley-VCH Verlag GmbH & Co. KGaA, Weinheim

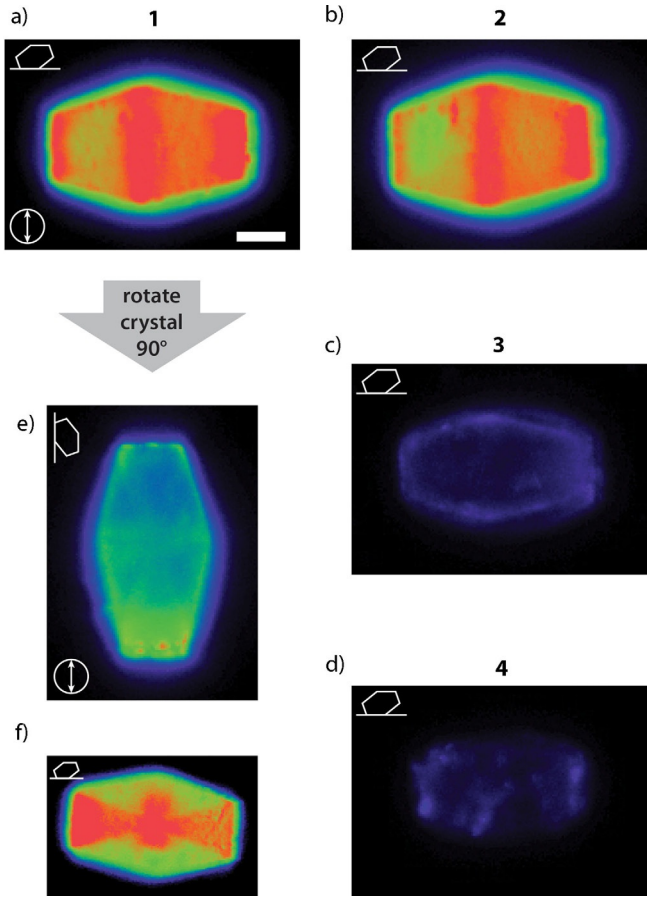

Figure 6. Fluorescence location in zeolite BEA crystals after staining with probes **1**–**4**. The experimental settings were kept constant for all CFM images in this figure except f). a–d) Summed intensity over all layers of 3D maps of the crystals stained with **1** (a), **2** (b), **3** (c), and **4** (d). The scale bar is 5 μm. e) Image of a zeolite BEA crystal after the crystal has been physically rotated by 90°, that is, with respect to the angle of polarization of the incoming laser light, showing diminished fluorescence intensity. f) Middle section of a zeolite BEA crystal showing the hourglass pattern observed after staining with a low amount of probe. The color scale of this CFM image was adjusted to show the hourglass pattern more clearly.

but with relatively large differences in fluorescence intensity. Because probe molecule **4** can only enter imperfections in the crystal, the heterogeneity in fluorescence is caused by the variations in the amount of imperfections in each crystal, which can be seen in Figure S2. With higher fluorescence intensity, fluorescence from cracks does not play a role, as evidenced by the results of probe molecules **1**–**3**. Furthermore, statistical analysis of the sets of fluorescence intensity showed that there were significant differences (>95% confidence) in intensity between sets of zeolite crystals stained with each of these probes (Table S1 in the Supporting Information).

Staining with a lower concentration of probe molecule **1** revealed an hourglass pattern for the BEA crystals (Figure 6 f), similar to the one observed in MFI crystals (Figure 4). This phenomenon has been observed before in large BEA crystals with the same morphology using crossed polarizers and is depicted here in small BEA crystals for the first time.[34] It is therefore likely that this is a general feature of BEA crystals with this morphology. Our results show that probe molecule **1**, when supplied in low amounts, preferentially enters the pyramidal subunits of the crystal. This is an indication that these subunits are imperfect because there are no straight pores opening to the square faces on the short edge of the crystal (see Figure 1 f). Furthermore, the large difference in intensity shows that internal diffusion barriers exist between the two pyramidal and the other subunits of the BEA crystals.

Zeolite BEA crystals stained with these probes all show a relatively high fluorescence intensity at the short edges of the crystal, that is, the base of the two pyramidal subunits (see Figure 6). It has been observed before that this face of the BEA crystals has a "rugged" structure with terraces with a height of 100–200 nm covering the surface.[34] Therefore, it is possible that this rugged structure is an indication of imperfections in or damage to these faces of the crystal, which allow probes of any size to enter the edge of the crystal easily. Moreover, the surface area of these faces is expected to be high. Polarization-dependent CFM measurements of the BEA crystals, which are shown in Figure 6 e and Figure S3 in the Supporting Information, allowed a deeper inquiry into the increased intensity at the short edges. Analogous to the MFI crystals, a 90° rotation of the zeolite crystals with respect to the polarization of the laser light leads to a diminished fluorescence intensity throughout most of the zeolite crystal. However, the short edges of the crystal still show a significant amount of fluorescence after rotation. This is in line with the hypothesized damage to the crystal on these faces, which allows probes to orient themselves more freely because the normal pore structure has been disrupted.[34] Rotation of the BEA crystal with 15° intervals results in the fluorescence intensity again giving a sin(2Θ) curve, consistent with the results for MFI crystals (Figure 7). These results confirm that probe molecules are

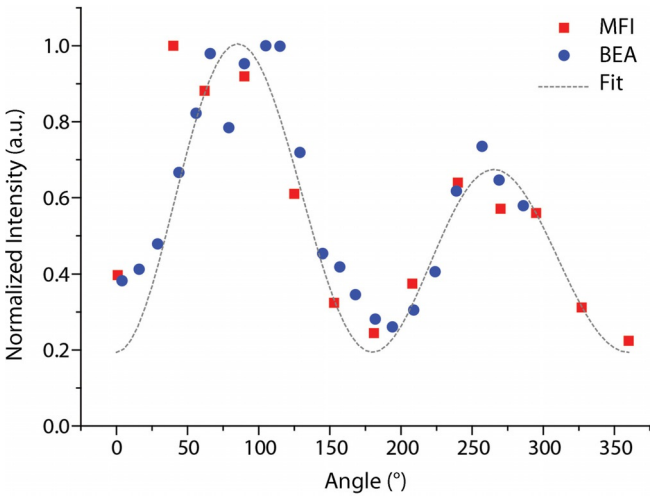

Figure 7. Intensity of fluorescence of probe molecule **1** within a zeolite MFI crystal (summed over the whole crystal) and a zeolite BEA crystal (intensity of middle plane) with respect to the angle of polarization. The angle was adjusted by physically rotating the crystal on the microscope table. The grey line represents a fit using a *exp(-Θ*c)*sin(2Θ)+b. Fit parameters were determined empirically. A decay of the intensity at higher angles (i.e., after longer laser exposure) is observed due to photo-bleaching of the probe molecules within the zeolite.

© 2017 The Authors. Published by Wiley-VCH Verlag GmbH & Co. KGaA, Weinheim

aligned within the pore system of these crystals and that fluorescence intensity can therefore be used to elucidate the direction of the micropores in (subunits of) the BEA crystals.

It has been previously reported from XRD measurements of very large BEA crystals that the [100] and [010] faces are on the long sides of the crystal. Thus, the straight pores are open to the long edges, whereas the sinusoidal pores are open at the short edges (i.e., the square-shaped faces).[34] The crystals can be observed lying on a surface in three different orientations: on the short-truncated end (rarely seen), or one of the four sides, leading to two observable orientations (opposing sides result in the same orientation). Unlike MFI with its roof and gable positions, the orientations of BEA lying on its side are indistinguishable (symmetrical). Because there are no significant differences in fluorescence intensity among the crystals stained with **1** (Figure S2), the two orientations must be equivalent. Therefore, the orientation of both straight pores of zeolite BEA is perpendicular to the long axis of the crystal and the sinusoidal pores run along the long axis of the crystal, which is in agreement with previous results.[34,35]

Conclusion

A new approach to assess the accessibility and pore structure of zeolite crystals has been successfully applied to study large crystals of MFI and BEA. It is found that in MFI crystals with a 90° intergrowth structure, the rotated subunits are prone to develop imperfections during crystal growth. The probe series used in these experiments, based on the fluorescent DAMPI scaffold with increasing molecular dimensions, can stain these cracks and zeolite imperfections, showing the relative extent of imperfections and damage in the zeolite crystals under study. The results of the adsorption of the distinct DAMPI-type probes can be quantified by CFM and provide a quantitative measure of accessibility for these crystals based on the uptake of the fluorescent probe molecules. Polarization-dependent CFM measurements show that although the cracks and imperfections are responsible for the macro-distribution, the probes are still aligned to the pore system of the crystal, with the larger probes presumably inserted end-on into the zeolite pore mouth, in a "stopcock" fashion.

Furthermore, the developed approach with DAMPI-type probes is applied successfully to the much less studied BEA zeolite crystals. The hourglass pattern, as observed in large BEA crystals, was observed for the first time in smaller BEA crystals, which makes it likely this is a general feature of BEA crystals of this morphology. Internal diffusion barriers between the subunits of a BEA crystal exist, which restrict probe movement. Polarization-dependent CFM measurements show imperfections exist on the short square ends of the crystal, which accommodate probes with no preferential orientation. Furthermore, evidence is provided that the pore orientation proposed in previous studies is correct; that is, the straight pores run perpendicular to the long axis of the BEA crystal.

In summary, investigating zeolite crystals using this series of DAMPI-type probes—with discrete molecular dimensions and which do not require external activation by light or an acidic site—offers a versatile and powerful tool to probe the accessibility of a wide variety of zeolite crystals. Furthermore, the methodology can visualize crystal imperfections, as well as internal diffusion barriers of zeolite crystals. The probes can therefore be used to evaluate how many imperfections are present within a specific crystal due to the synthesis method or subsequent calcination steps. The current study suggests that BEA crystals have intrinsically less structural imperfections than MFI crystals, which is in line with what is expected based on the synthesis method. Furthermore, polarization-dependent CFM measurements can be used in combination with these probe molecules to elucidate pore network directions within zeolite crystals.

Experimental Section

CFM measurements and mapping were performed on a Nikon Eclipse 90i upright microscope using a 100x/0.70 NA dry objective. The microscope is equipped with a Nikon-Eclipse A1R scan head. CFM images were recorded using excitation from a Melles Griot Argon ion 488 nm laser providing 40 mW. The extinction ratio of the polarization for this laser is >250:1. Fluorescence emitted from MFI crystals was detected by a single photomultiplier using a 525/50 band pass filter, whereas fluorescence emitted from BEA crystals was detected by a spectral detection unit equipped with a diffraction grating and a 32 photomultiplier tube array (detection in the range of 518–710 nm). Scanning electron microscopy (SEM) images of MFI crystals were acquired on a Phenom SEM (Phenom World) equipped with a CsB6 filament at 5 kV in backscatter electron (BSE) mode. SEM images of BEA crystals were acquired on a ZEISS 1550 VP FESEM, equipped with in-lens SE. Ludox AS-40 (40 wt% in H_2O), zinc fluoride (99.999%), and pyridine (>99%) were purchased from Aldrich. 4-(4-Diethylaminostyryl)-1-methylpyridinium iodide **2** (98%) and tetrapropylammonium bromide (>99%) were purchased from Fluka. Aluminium sulphate octadecahydrate (98%) and ammonium hydroxide (28–30%) were purchased from J. T. Baker. Tetraethylammonium fluoride hydrate (97%) was purchased from Alfa Aesar, whereas Cabosil M-5 was purchased from Cabot Corporation. The synthesis of probe **1**, **3**, and **4** has been described in detail elsewhere.[28]

The zeolite MFI crystals were provided by ExxonMobil and have a Si/Al ratio of 17. Details on these crystals have been reported in previous work from our group.[19,22] The synthesis gel had a molar composition of $6.65\,(NH_4)_2O/0.67\,TPA_2O/0.025\,Al_2O_3/10\,SiO_2/121\,H_2O$. The gel was, without agitation, heated from RT to 453 K in 2 h. The crystals were kept at 453 K for 168 h. The MFI crystals were first calcined in air to remove the template. The temperature was increased at 1 K min^{-1} to 523 K and held for 2 h. The temperature was then increased at 1 K min^{-1} to 773 K and held for 12 h. Afterwards, the temperature was decreased at 1 K min^{-1} to RT. Crystals were ion-exchanged three times using a 10% solution of NH_4NO_3 at 333 K for 24 h. A final calcination was carried out using the same program as for template removal. The zeolite BEA crystals used were synthesized in a non-aqueous system, similar to that used by Kuperman et al. to synthesize a number of large zeolite crystals, most notably giant crystals of ferrierite.[48] First, 6.55 g of pyridine was mixed with 1.05 g of tetraethylammonium fluoride dehydrate, 0.074 g of $ZnF_2{\cdot}4\,H_2O$ and 6.55 g of pyridine. Then 2 g of water was added to obtain a clear solution. Finally, 0.5 g of Cabosil was added and mixed by hand until a homogenous gel was obtained. Final molar ratios were $1\,SiO_2/0.03\,ZnF_2/0.65$ TEAF/10 Pyri-

 © 2017 The Authors. Published by Wiley-VCH Verlag GmbH & Co. KGaA, Weinheim

dine/15 H_2O. The mixture was placed in a 23 mL Parr reactor and placed in a tumbling oven at 413 K for 24 days. The crystals were recovered by centrifugation and were rinsed with water several times followed by a final wash with acetone and then dried in air at 373 K. The BEA crystals were calcined in air. The temperature was increased at 1 K min^{-1} to 423 K and held at this temperature for 3 h, then heated to 853 K at 1 K min^{-1} and held at this temperature for 6 h.

Immediately prior to staining experiments, the zeolite crystals were calcined in air. The temperature was increased at 1 K min^{-1} to 523 K and held at this temperature for 2 h. The temperature was then increased at 1 K min^{-1} to 773 K and held at this temperature for 6 h. Afterwards, the temperature was decreased at 1 K min^{-1} until 373 K, at which the container with the crystals was sealed to minimize adsorption of water before cooling to RT. Both MFI and BEA crystals were stained with a concentration of 1 μM for all probes, unless otherwise indicated. These suspensions were allowed to stand for one week; if the crystal were standing for a longer time, no additional fluorescence intensity was observed. The crystals were not stirred to avoid damaging them. After staining, the crystals were either filtered using a PTFE 0.45 μm filter and, in the case of MFI, washed 3 times with ethanol, or washed by adding and siphoning off ethanol 3 times. Fluorescence of the zeolite crystals was evaluated by CFM. All crystals considered were of the same size. In quantification experiments, the "roof" orientation was used for MFI crystals. CFM maps of the crystals were created by stacking 23 slices of the crystal with a Z increment of 1 μm. The fluorescence intensity was summed over the whole stack and the background fluorescence, taken from the same image, was subtracted. The results for each probe were divided by the extinction coefficient to correct for differences in absorption efficiency between probes. Although the stained zeolite crystals were kept in a desiccator to minimize exposure to contaminants, MFI crystals that were kept for longer than one month after staining were often found to be contaminated with a fluorescent species accumulating at the edges of the crystal. Fortunately, this contamination could be detected by anomalies in the emission spectrum. In polarization-dependent CFM experiments, the intensities of the fluorescence of both type of crystals were evaluated at 15° (BEA) or 30° (MFI) intervals.

The anisotropy of light absorption by the probe molecules was investigated using real-time TDDFT. For simplicity, probe **1** was used for these calculations, as the alkyl substituents have no substantial influence on the photo-physical properties of the conjugated system. The molecular geometry was optimized on the ground state energy surface using DFT at the B3LYP/6–311G level of theory. Convergence of the geometry optimization was confirmed by frequency calculations. To properly assess long-range charge transfer interactions between the pyridinium and the aniline moieties, the cam-B3LYP hybrid functional was used in the TDDFT calculations. The RT-TDDFT simulation of absorption anisotropy was performed by evolving the density matrix in response to a polarized external electric field aligned to the molecular axes as described by Lopata et al.[49].

Acknowledgements

The authors wish to thank Dr. Florian Meirer (Utrecht University, UU) for help with the data analysis. Dr. Javier Ruiz-Martínez (UU), Dr. Joost van der Lit (UU) and Dr. Zoran Ristanović (UU) are acknowledged for useful discussions, whereas Özgün Attila (UU) is acknowledged for providing the MFI crystal SEM images. This work is financially supported by a Top grant of CW-NWO. J.S. has received funding from the European Union's Horizon 2020 research and innovation programme under the Marie Sklodowska-Curie grant agreement No 702149. Dr. Machteld Mertens (ExxonMobil) and Prof. Mark E. Davis (California Institute of Technology) are acknowledged for providing the MFI and BEA crystals, respectively.

Conflict of interest

The authors declare no conflict of interest.

Keywords: confocal fluorescence microscopy · crystal growth · fluorescent probes · polarization dependence · zeolites

[1] C. Martínez, A. Corma, *Coord. Chem. Rev.* **2011**, *255*, 1558 – 1580.
[2] E. T. C. Vogt, G. T. Whiting, A. Dutta Chowdhury, B. M. Weckhuysen, *Adv. Catal.* **2015**, *58*, 143 – 314.
[3] W. Vermeiren, J.-P. Gilson, *Top. Catal.* **2009**, *52*, 1131 – 1161.
[4] E. Taarning, C. M. Osmundsen, X. Yang, B. Voss, S. I. Andersen, C. H. Christensen, *Energy Environ. Sci.* **2011**, *4*, 793 – 804.
[5] P. A. Jacobs, M. Dusselier, B. F. Sels, *Angew. Chem. Int. Ed.* **2014**, *53*, 8621 – 8626; *Angew. Chem.* **2014**, *126*, 8765 – 8770.
[6] T. Ennaert, J. Van Aelst, J. Dijkmans, R. De Clercq, W. Schutyser, M. Dusselier, D. Verboekend, B. F. Sels, *Chem. Soc. Rev.* **2016**, *45*, 584 – 611.
[7] B. Smit, T. L. M. Maesen, *Chem. Rev.* **2008**, *108*, 4125 – 4184.
[8] U. Olsbye, S. Svelle, M. Bjørgen, P. Beato, T. V. W. Janssens, F. Joensen, S. Bordiga, K. P. Lillerud, *Angew. Chem. Int. Ed.* **2012**, *51*, 5810 – 5831; *Angew. Chem.* **2012**, *124*, 5910 – 5933.
[9] S. C. C. Wiedemann, Z. Ristanović, G. T. Whiting, V. R. Reddy Marthala, J. Kärger, J. Weitkamp, B. Wels, P. C. A. Bruijnincx, B. M. Weckhuysen, *Chem. Eur. J.* **2016**, *22*, 199 – 210.
[10] K. Liu, A. V. Kubarev, J. Van Loon, H. Uji-i, D. E. De Vos, J. Hofkens, M. B. J. Roeffaers, *ACS Nano* **2014**, *8*, 12650 – 12659.
[11] K. F. Domke, T. A. Riemer, G. Rago, A. N. Parvulescu, P. C. A. Bruijnincx, A. Enejder, B. M. Weckhuysen, M. Bonn, *J. Am. Chem. Soc.* **2012**, *134*, 1124 – 1129.
[12] G. Calzaferri, *Langmuir* **2012**, *28*, 6216 – 6231.
[13] G. Tabacchi, E. Fois, G. Calzaferri, *Angew. Chem. Int. Ed.* **2015**, *54*, 11112 – 11116; *Angew. Chem.* **2015**, *127*, 11264 – 11268.
[14] C. Sprung, B. M. Weckhuysen, *J. Am. Chem. Soc.* **2015**, *137*, 1916 – 1928.
[15] J. P. Hofmann, D. Mores, L. R. Aramburo, S. Teketel, M. Rohnke, J. Janek, U. Olsbye, B. M. Weckhuysen, *Chem. Eur. J.* **2013**, *19*, 8533 – 8542.
[16] G. Muller, T. Narbeshuber, G. Mirth, J. A. Lercher, *J. Phys. Chem.* **1994**, *98*, 7436 – 7439.
[17] M. B. J. Roeffaers, R. Ameloot, M. Baruah, H. Uji-i, M. Bulut, G. De Cremer, U. Müller, P. A. Jacobs, J. Hofkens, B. F. Sels, D. E. De Vos, *J. Am. Chem. Soc.* **2008**, *130*, 5763 – 5772.
[18] P. Kortunov, S. Vasenkov, C. Chmelik, J. Kärger, D. M. Ruthven, J. Wloch, *Chem. Mater.* **2004**, *16*, 3552 – 3558.
[19] L. Karwacki, M. H. F. Kox, D. A. M. de Winter, M. R. Drury, J. D. Meeldijk, E. Stavitski, W. Schmidt, M. Mertens, P. Cubillas, N. John, A. Chan, N. Kahn, S. R. Bare, M. Anderson, J. Kornatowski, B. M. Weckhuysen, *Nat. Mater.* **2009**, *8*, 959 – 965.
[20] M. Busby, H. Kerschbaumer, G. Calzaferri, L. De Cola, *Adv. Mater.* **2008**, *20*, 1614 – 1618.
[21] K. S. W. Sing, R. T. T. Williams, *Part. Part. Syst. Charact.* **2004**, *21*, 71 – 79.
[22] Z. Ristanović, J. P. Hofmann, M.-I. Richard, T. Jiang, G. A. Chahine, T. U. Schülli, F. Meirer, B. M. Weckhuysen, *Angew. Chem. Int. Ed.* **2016**, *55*, 7496 – 7500; *Angew. Chem.* **2016**, *128*, 7622 – 7626.
[23] M. H. F. Kox, K. F. Domke, J. P. R. Day, G. Rago, E. Stavitski, M. Bonn, B. M. Weckhuysen, *Angew. Chem. Int. Ed.* **2009**, *48*, 8990 – 8994; *Angew. Chem.* **2009**, *121*, 9152 – 9156.
[24] Z. Ristanović, J. P. Hofmann, G. De Cremer, A. V. Kubarev, M. Rohnke, F. Meirer, J. Hofkens, M. B. J. Roeffaers, B. M. Weckhuysen, *J. Am. Chem. Soc.* **2015**, *137*, 6559 – 6568.

 © 2017 The Authors. Published by Wiley-VCH Verlag GmbH & Co. KGaA, Weinheim

[25] M. B. J. Roeffaers, R. Ameloot, A.-J. Bons, W. Mortier, G. De Cremer, R. de Kloe, J. Hofkens, D. E. De Vos, B. F. Sels, *J. Am. Chem. Soc.* **2008**, *130*, 13516 – 13517.
[26] E. Stavitski, M. R. Drury, D. A. M. De Winter, M. H. F. Kox, B. M. Weckhuysen, *Angew. Chem. Int. Ed.* **2008**, *47*, 5637 – 5640; *Angew. Chem.* **2008**, *120*, 5719 – 5722.
[27] M. H. F. Kox, E. Stavitski, B. M. Weckhuysen, *Angew. Chem. Int. Ed.* **2007**, *46*, 3652 – 3655; *Angew. Chem.* **2007**, *119*, 3726 – 3729.
[28] F. C. Hendriks, D. Valencia, P. C. A. Bruijnincx, B. M. Weckhuysen, *Phys. Chem. Chem. Phys.* **2017**, *19*, 1857 – 1867.
[29] IZA, *Database of Zeolite Structures*, Retrieved: 2 August, **2016**.
[30] L. R. Aramburo, L. Karwacki, P. Cubillas, S. Asahina, D. A. M. de Winter, M. R. Drury, I. L. C. Buurmans, E. Stavitski, D. Mores, M. Daturi, P. Bazin, P. Dumas, F. Thibault-Starzyk, J. A. Post, M. W. Anderson, O. Terasaki, B. M. Weckhuysen, *Chem. Eur. J.* **2011**, *17*, 13773 – 13781.
[31] Y. S. S. Lin, N. Yamamoto, Y. Choi, T. Yamaguchi, T. Okubo, S.-I. I. Nakao, *Microporous Mesoporous Mater.* **2000**, *38*, 207 – 220.
[32] M. Moliner, Y. Román-leshkov, M. E. Davis, Y. Roman-Leshkov, M. E. Davis, *Proc. Natl. Acad. Sci. USA* **2010**, *107*, 6164 – 6168.
[33] R. Gounder, *Catal. Sci. Technol.* **2014**, *4*, 2877 – 2886.
[34] J. Sun, G. Zhu, Y. Chen, J. Li, L. Wang, Y. Peng, H. Li, S. Qiu, *Microporous Mesoporous Mater.* **2007**, *102*, 242 – 248.
[35] A. N. Parvulescu, D. Mores, E. Stavitski, C. M. Teodorescu, P. C. A. Bruijnincx, R. J. M. K. Gebbink, B. M. Weckhuysen, *J. Am. Chem. Soc.* **2010**, *132*, 10429 – 10439.
[36] M. Tong, D. Zhang, W. Fan, J. Xu, L. Zhu, W. Guo, W. Yan, J. Yu, S. Qiu, J. Wang, F. Deng, R. Xu, *Sci. Rep.* **2015**, *5*, 11521.
[37] R. Szostak, J. M. Pan, K. P. Lillerudo, *J. Phys. Chem.* **1995**, *99*, 2104 – 2109.
[38] R. Szostak, K. P. Lillerud, M. Stocker, *J. Catal.* **1994**, *148*, 91 – 99.
[39] J. M. Newsam, M. M. J. Treacy, W. T. Koetsier, C. B. D. Gruyter, *Proc. R. Soc. A Math. Phys. Eng. Sci.* **1988**, *420*, 375 – 405.
[40] D. Guillaumont, S. Nakamura, *Dye. Pigment.* **2000**, *46*, 85 – 92.
[41] J. R. Agger, N. Hanif, C. S. Cundy, A. P. Wade, S. Dennison, P. A. Rawlinson, M. W. Anderson, *J. Am. Chem. Soc.* **2003**, *125*, 830 – 839.
[42] J. Lu, E. Bartholomeeusen, B. F. Sels, D. Schrijvers, *J. Microsc. (Oxford, U. K.)* **2016**, *264*, 370 – 377.
[43] J. C. Saint Remi, A. Lauerer, C. Chmelik, I. Vandendael, H. Terryn, G. V. Baron, J. F. M. Denayer, J. Kärger, *Nat. Mater.* **2015**, *15*, 401 – 406.
[44] R. A. Ocakoglu, J. F. M. Denayer, G. B. Marin, J. A. Martens, G. V. Baron, *J. Phys. Chem. B* **2003**, *107*, 398 – 406.
[45] A. R. Teixeira, C.-C. Chang, T. Coogan, R. Kendall, W. Fan, P. J. Dauenhauer, *J. Phys. Chem. C* **2013**, *117*, 25545 – 25555.
[46] M. H. F. Kox, E. Stavitski, J. C. Groen, J. Pérez-Ramírez, F. Kapteijn, B. M. Weckhuysen, *Chem. Eur. J.* **2008**, *14*, 1718 – 1725.
[47] C. Weidenthaler, R. X. Fischer, R. D. Shannon, O. Medenbach, *J. Phys. Chem.* **1994**, *98*, 12687 – 12694.
[48] A. Kuperman, S. Nadimi, S. Oliver, G. A. Ozin, J. M. Garcés, M. M. Olken, *Nature* **1993**, *365*, 239 – 242.
[49] K. Lopata, N. Govind, *J. Chem. Theory Comput.* **2011**, *7*, 1344 – 1355.

Manuscript received: January 6, 2017
Accepted Article published: February 19, 2017
Final Article published: March 20, 2017

 © 2017 The Authors. Published by Wiley-VCH Verlag GmbH & Co. KGaA, Weinheim